The Potential of Deriving Tree-Ring-Based Field Reconstructions of Droughts and Pluvials over Fennoscandia*,+

KRISTINA SEFTIGEN

Regional Climate Group, Department of Earth Sciences, University of Gothenburg, Gothenburg, Sweden

EDWARD R. COOK

Lamont-Doherty Earth Observatory, Palisades, New York

HANS W. LINDERHOLM, MAURICIO FUENTES, AND JESPER BJÖRKLUND

Regional Climate Group, Department of Earth Sciences, University of Gothenburg, Gothenburg, Sweden

(Manuscript received 2 December 2013, in final form 16 October 2014)

ABSTRACT

Moisture availability has been identified as one of the most important factors in the context of future climate change. This paper explores the potential of applying a multiproxy approach to dendroclimatology to infer the twentieth-century moisture variability over Fennoscandia. Fields of the warm-season (June–August) standardized precipitation evapotranspiration index (SPEI) were developed from a dense network of precipitation-sensitive annually resolved tree-ring width (TRW), maximum density (MXD), and stable carbon (δ^{13}C) and oxygen (δ^{18}O) isotope chronologies using a point-by-point local regression technique (PPR). Two different approaches were tested for selecting candidate tree-ring predictors of SPEI for each gridpoint reconstruction: a search radius method and a search spatial correlation contour method. As confirmed by a range of metrics of reconstruction fidelity, both methods produced reconstructions showing a remarkably high accuracy in a temporal sense, but with some minor regional differences. As a whole, the spatial skill of the reconstructed fields was generally quite good, showing the greatest performance in the central and southern parts of the target region. Lower reconstruction skills were observed in northern part of the study domain. Regional-scale moisture anomalies were best captured by the reconstructions, while local-scale features were not as well represented. The authors speculate that a spatially and temporally varying tree-ring proxy response to temperature and precipitation in the region may cause some uncertainties in a Fennoscandian hydroclimatic reconstruction; this needs further investigation. Overall, this study shows a great potential for making long-term spatiotemporal reconstructions of moisture variability for the Fennoscandian region using tree-ring data.

---

1. Introduction

Observations of increased global temperatures, reduction in ice and snow covers, and rising global sea level are all unambiguous evidences of a warming climate system. It is well recognized that the global mean surface temperature has increased during the past century (e.g., Hansen et al. 2010; Lawrimore et al. 2011; Jones et al. 2012; Rohde et al. 2013), and, according to future climate projections, will continue to rise over the twenty-first century (IPCC 2013). A warmer climate will lead to an increased risk of hydroclimatological extremes (Wetherald and Manabe 2002). While northern Europe has already shown

a 10%–40% increase in precipitation over the twentieth century, projections indicate that mean rainfall and intensity will continue to increase in mid and high latitudes (Meehl et al. 2005). Annual average runoff is projected to increase in northern Europe with up to 22% until the 2070s (Alcamo et al. 2007), and an increase in rainfall amounts and intensities is likely to lead to increased risks of flooding (EEA 2004). Flood events not only pose a fundamental threat to human life and property but may also have a significant impact on the natural environment. Increased rainfall intensity will affect the water quality through greater rates of erosion (Rumsby and Macklin 1994), an increased soil washout and spread of pollutants and fertilizers (Fisher 2000; Boorman 2003), and an intensified acidification of water bodies as a result of increased atmospheric deposition (Ferrier and Edwards 2002; Gilvear et al. 2002; Soulsby et al. 2002). It is apparent that climate variability and change already pose a challenge to Europe's economic sectors, production systems, and ecosystems. Given the future climate projections there is a great need to prepare for an intensification of these impacts.

To be able to assess the possible implications of future changes in the hydrological cycle, and be able to plan and mitigate the impacts of related extremes, firm knowledge about past natural moisture variability is needed. This includes an understanding of both the temporal nature and spatial characteristics of extreme moisture events, and the factors controlling them. Data from trees growing under harsh climatic conditions can be used as powerful, annually resolved, proxies of past climatic events, such as drought or floods (Fritts 2001). The wide geographical distribution of tree-ring chronologies offers the potential not only to reconstruct local climate variability, but also to infer past large-scale climatic patterns. Recently, two successful attempts have been made to reconstruct ''atlases'' of past moisture variability from densely sampled networks of moisture-sensitive tree-ring chronologies: the North American Drought Atlas (NADA; Cook et al. 1999, 2004) and the Monsoon Asia Drought Atlas (MADA; Cook et al. 2010). These reconstructions have not only provided valuable information of past hydroclimatic characteristics (e.g., understanding of major drought regions and the severity, frequency, and general footprint of major droughts), but have also revealed the occurrence of past, previously unknown, megadroughts over North America and Southeast Asia, respectively. Moreover, the NADA has contributed essential background data for unraveling the underlying mechanisms of North American drought variability, such as the key role of tropical Pacific Ocean, and also indications of the importance of the North Pacific and Atlantic Ocean as controls on the regional drought patterns (e.g., Herweijer et al. 2007; Cook et al. 2007; Woodhouse et al. 2009).

Tree-ring data from the Fennoscandian region have previously been considered of limited use in reconstructing past hydroclimatic conditions (Erlandsson 1936; Eklund 1954). This is because tree growth in moist and cool environments is generally not limited by precipitation, but rather reflects the thermal conditions of the surrounding environment. Hence, in the Nordic countries a great deal of research has been focused on developing temperature-sensitive tree-ring width, maximum latewood density, and, to a lesser extent, tree-ring $\delta^{13}C$ and $\delta^{18}O$ chronologies, to infer past temperature variability (Linderholm et al. 2010). Comparatively few efforts have been made to provide tree-ring-based hydroclimatological reconstructions for this region (Helama and Lindholm 2003; Linderholm et al. 2004; Linderholm and Molin 2005; Helama et al. 2009; Jönsson and Nilsson 2009; Drobyshev et al. 2011; Seftigen et al. 2013) and, up to this point, no attempts to make tree-ring-based gridded moisture reconstructions for the Fennoscandian region have yet been made.

The aim of this study was to assess the potential of using tree-ring data from Fennoscandia to make a spatiotemporal reconstruction of past moisture variability, as expressed by the standardized precipitation evapotranspiration index (SPEI). When using a proxy to reconstruct past climate, the potential of the proxy is usually measured through the strength of the linear correlation between the measured proxy and the climate parameter. There is, however, no clear guidance in the literature as to how strong the linear relationship must be. Here we applied a range of calibration and validation diagnostic approaches commonly used in dendroclimatic reconstruction to assess the spatial reconstruction performance. The feasibility of using a point-by-point regression approach (PPR), the same reconstruction methodology previously used in the NADA and MADA, to produce past moisture variability patterns for the region was explored. Previous studies have shown that by combining multiple tree-ring parameters tuned to the same dominant environmental control, it may be possible to produce reconstructions that are more accurate than those derived from a single tree-ring variable (Gagen et al. 2004, 2006; McCarroll et al. 2003, 2011, 2013). Hence, the objective of the current study was to apply a multiparameter approach to dendroclimatology in order to infer information about twentieth-century moisture variability.

2. Data and methods

a. Study region

The study region covers Norway, Sweden, and Finland, and is located within 55°20'–71°11'N and 4°29'–31°35'E. The climate in the area is strongly influenced

by the adjacent North Atlantic Ocean and the heterogeneous topography of the region (altitude range from sea level to 2217 m above sea level (Fig. 1a). The Scandinavian Mountains range, which runs in a southwest–northeast direction through Norway and the central and northern parts of western Sweden, separates the maritime area to the west from a more continental area in the east. The highest annual precipitation is found along the Norwegian coast, where locally the total annual precipitation may reach 2500 mm or more, and on the windward west side of the mountain range where a release of orographic precipitation is caused by the forced uplift of approaching air masses (Smith 1979; Fig. 1b). The eastern leeward side of the mountain divide is drier and has a more pronounced continental climate. The influence of continentality generally increases toward the east-northeast, with a slight decrease around the Baltic Sea and toward the Arctic Ocean in the north (Fig. 1c). The atmospheric circulation is the main forcing for the regional climate variability. Busuioc et al. (2001) identified three main large-scale circulation mechanisms controlling the Swedish spatial rainfall variability: 1) the North Atlantic Oscillation (NAO) representing a westerly (easterly) flow and causing positive (negative) anomalies over the entire region, 2) cyclonic (anticyclonic) structure centered generally over the British Isles and leading to positive (negative) precipitation anomalies over almost the entire region, and 3) a west–east monthly sea level pressure dipole structure causing ether a north–south or west–east gradient in rainfall depending on the position and extension of the pressure anomalies. Convective rainfall mainly occurs in the warm season, while frontal rainfall is more important in winter compared to summer (Hofstra and New 2009). Late summer to autumn is the time of the most abundant rainfall in the region (Fig. 1d).

b. Tree-ring network

Twenty-three new Scots pine (*Pinus sylvestris* L.) tree-ring chronologies were collected from southern and central Sweden for the purpose of reconstructing past hydroclimatic conditions. The sites are mostly located in a transition zone between the boreal and temperate biomes, and so both coniferous and deciduous trees are common elements of the vegetation. The individual sampling sites were selected to maximize the moisture signal in the tree growth. Bare rocks and thin, nutrient-poor soil layers with limited water holding capacity characterize these sites. The vegetation is dominated by a dry Scots pine forest with scattered Norway spruce (*Picea abies* Karst) and downy birch (*Betula pubescens* Ehrh.) and aspen (*Populus tremula* L.) in the more mesic parts of the terrain. The sparse field layer has typically

a low species diversity and is dominated by various dwarf-shrubs, such as *Vaccinium* spp. and *Empetrum* spp. All the sites showed more or less noticeable signs of agrarian colonization, modern forest exploitation, and human collecting activities. Logging on a larger scale took place throughout the country in the late nineteenth century, whereupon much of the forested areas were cleaned of dead and diseased trees. A major obstacle for compiling long tree-ring chronologies in the region is thus the low abundance of dead wood and old trees. The strategy of the current study was to increase the number of moisture-sensitive tree-ring chronologies throughout southern and central Sweden, and to focus the sampling on living trees only. Two cores from each tree were extracted using an increment borer. The number of trees sampled varied between 20 and 50 trees per site, covering all age classes. The samples were prepared and cross-dated according to standard dendrochronological procedures (Stokes and Smiley 1968), and the width of each annual ring was measured to the nearest 0.001 mm.

In addition to the newly sampled chronologies, virtually all available chronologies from the study area were downloaded from the International Tree-Ring Data Bank (ITRDB; www.ncdc.noaa.gov/paleo/treering.html; Grissino-Mayer and Fritts 1997). Data that were not downloaded included chronologies of questionable quality and/or with a temporal coverage outside the period targeted by this study. In addition to the ITRDB downloaded data, many chronologies were kindly contributed by colleagues. A network containing 156 chronologies was retained for the analysis, including annually resolved tree-ring width (TRW), maximum density (MXD), and stable carbon ($\delta^{13}C$) and oxygen ($\delta^{18}O$) isotope chronologies from Scots pine, Norway spruce (*Picea abies* L.), and pedunculate oak (*Quercus robur* L.). A large number of the ITRDB downloaded chronologies have an ending year around 1970–80. The time domain of the current study was therefore restricted to the 1901–76 period, which is the time period common for the tree-ring and climate data.

The focus of this study was to assess the potential of tree-ring data to estimate regional moisture variations on the interannual to decadal scale, which is why analyses only dealt with the high-frequency portion of data. Most of the low-frequency information, related to multidecadal or longer-term trends, was removed from the tree-ring data through standardization. This was accomplished by fitting a 35-yr cubic smoothing spline with 50% frequency-response cutoff to each individual series (Cook and Peters 1981), and then dividing (or in the case of MXD, subtracting) the tree-ring data by the corresponding value of the fitted spline for each year. The
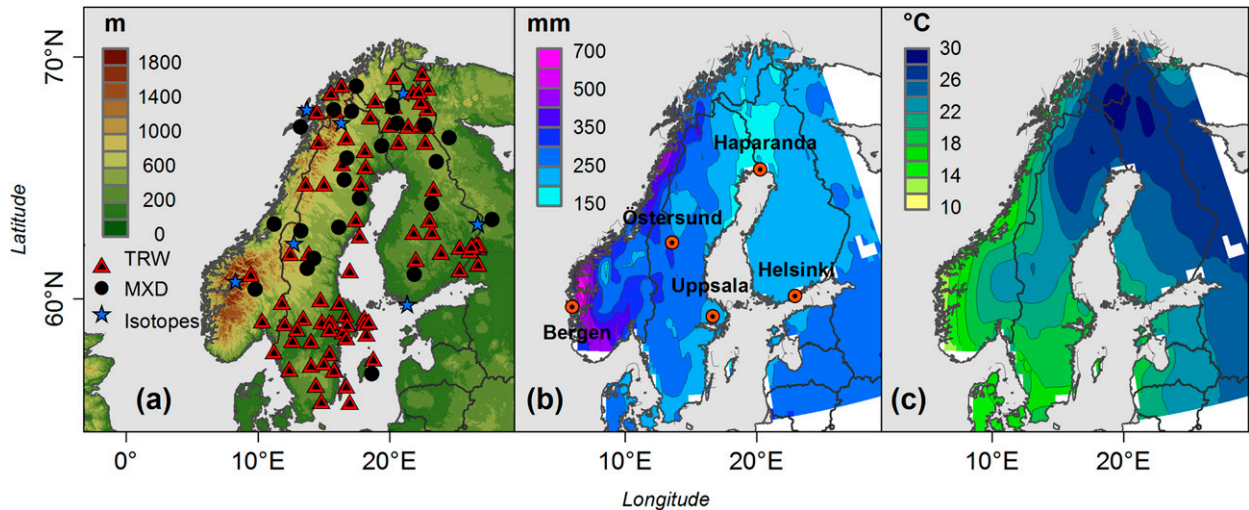
FIG. 1. (a) Location of the tree-ring network sites, superimposed on a topographical map over the study region, (b) May–August precipitation totals, (c) continentality (defined here as the difference between July and January average temperatures), and (d) interannual distribution of monthly-mean temperature and total precipitation at selected climate stations [location shown in map in (b)]. Note that (b) and (c) are based on the CRU TS3 dataset over the 1901–2006 time period, and (d) is based on station data from the Nordklim database covering the period from 1890 to present.

resulting dimensionless series were averaged arithmetically into mean site chronologies.

c. Data selection

Precipitation is the main meteorological element influencing droughts and pluvials (Wilhite and Glantz 1985; Chang and Cleopa 1991; Heim 2002; Lloyd-Hughes and Saunders, 2002). Variables such as temperature, evapotranspiration, wind speed, and soil water holding capacity may also play an important role in determining the severity of dryness and wetness. Potential candidate tree-ring predictors for a hydroclimatic field reconstruction were therefore preselected based on the criteria requiring the tree-ring data to have a significant relationship (either positive or negative) with current year rainfall over a 6-month window, extending from April to September. All tree-ring chronologies were prescreened (referred to as screening 1) against instrumental temperature and precipitation data from the 0.5° × 0.5° CRU TS3.0 gridded dataset covering the 1901–2006 time period (Harris et al. 2013). Pearson correlation coefficients were calculated between each tree-ring chronology and climate data from the grid box centered on the chronology location, over the common 1902–76 period. The aim was to assess the relationship between growth and climate on an interannual time scale. Hence, both climate and tree-ring data were detrended by taking the first differences of the original data prior to the correlation analysis. The precipitation and temperature data for the study region showed, in general, a significant negative correlation during the

summer season. Because of this dependence, partial correlations were calculated between tree-ring variables and temperature (holding the precipitation constant) and precipitation (holding the temperature constant). The method described by Meko et al. (2011), and available as part of the MATLAB function seascorr, was used to obtain the confidence intervals for partial correlations. Using a Monte Carlo approach, each tree-ring chronology was simulated 1000 times by exact simulation (Percival and Constantine 2006), preserving the spectral properties of the series. Partial correlations were calculated between climate and simulated tree-ring data, and the empirical cumulative distribution functions of the resulting simulation-based partial correlations were used to establish two-sided 95% confidence intervals [see Meko et al. (2011) for details].

d. Climate field

A variety of quantitative measures have been developed for the purpose of defining and measuring wetness and dryness. Many tree-ring studies have successfully reconstructed drought indices such as the Palmer Drought Severity Index (PDSI; Palmer 1965; e.g., Stockton and Meko 1975, 1983; Cook and Jacoby 1977; Blasing and Duvick 1984; Cook et al. 1988, 1992; Meko 1992; Stahle et al. 1985, 1988; Cook et al. 1996), and/or, to a lesser extent, the standardized precipitation index (SPI; McKee et al. 1993; e.g., Linderholm and Molin 2005; Touchan et al. 2005; Seftigen et al. 2013; Levanič et al. 2013), the former being based on a soil water balance equation and the latter on a precipitation
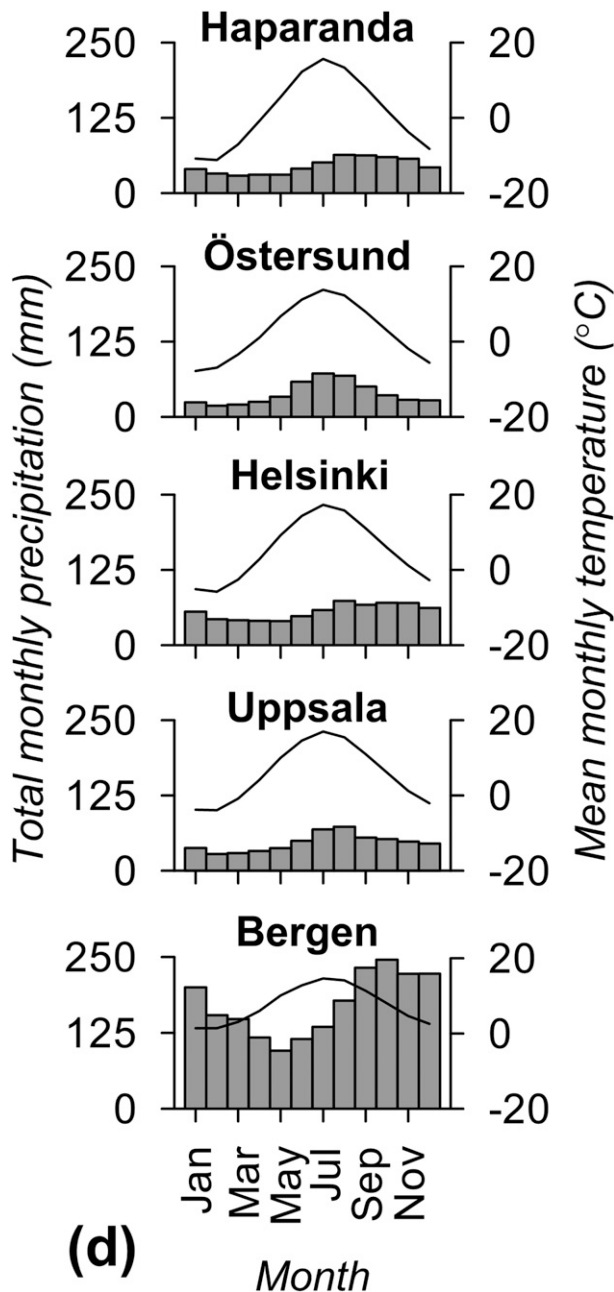
FIG. 1. (*Continued*)

probabilistic approach. Even though both indices have become widely accepted in drought monitoring and have been tested worldwide, each of them has its own shortcomings. SPI is based on precipitation data only, and does not consider other variables that may have an important influence on moisture availability. PDSI, on the other hand, includes both precipitation and temperature in its calculation (the latter one is used for estimation of evapotranspiration). Indices including temperature have been argued to be preferable over

precipitation-based indices, especially in applications dealing with future climate scenarios (Vicente-Serrano et al. 2010). PDSI, however, has proven most effective in determining long-term moisture anomalies. Yet, droughts and pluvials may occur over a range of time scales and the response time of different systems (agriculture, water resources, ecosystems, etc.) to the amount of water available varies widely. Another issue is that PDSI may contain an autoregressive component, so that the index for a given month may be affected by the moisture conditions during the preceding months or even the same months of several previous years (Guttman 1998).

The moisture index used in this study was the SPEI. Although SPEI is mathematically similar to SPI it also includes the effect of temperature variability on drought. Hence, under global warming conditions, SPEI is able to identify an increase in drought severity associated with higher water demand as a result of higher evapotranspiration. Moreover, relative to the PDSI, SPEI has the crucial advantage of being multi-scalar, allowing identification of different drought types. This quite recently developed index (Vicente-Serrano et al. 2010) has not, as far as we know of, previously been used in any dendroclimatological reconstructions. Data for this study were obtained from the global 0.5° gridded SPEI dataset spanning over the 1901–2006 time period (SPEIbase v1.0; http://sac.csic.es/spei/index.html). The target field for our hydroclimatic reconstruction consisted of 1391 grid points covering an area within 55°–73°N and 2°–33°E. Calculation of SPEI is based on similar computation methods as SPI, but includes both temperature and precipitation data. To get SPEI monthly differences (D) between precipitation and potential evapotranspiration (PET) are calculated and summarized over the time-scale of interest. SPEI is then obtained by fitting a log-logistic probability distribution function to data series of D and transforming it into a standardized normal distribution [see Vicente-Serrano et al. (2010) for details]. The resulting SPEI values commonly range between −2.5 and 2.5 (corresponding to exceedance probabilities of 0.006 and 0.994, respectively). Negative values correspond to dry conditions and positive values to wet conditions. The more the SPEI value deviates from zero, the larger is the departure from normal moisture conditions. Temperature and precipitation data used to obtain SPEIbase v1.0 came from the CRU TS3.0 dataset, and PET was calculated according the method proposed by Thornthwaite (1948). Although PET estimates based on Penman-type approaches are considered to be more physically realistic (Allen et al. 1994a,b), the purpose

of including PET in the SPEI calculation is to obtain a relative temporal estimation, and therefore the method used to compute PET is not crucial here (Vicente-Serrano et al. 2010). For example, Mavromatis (2007) recently showed that the use of simple or complex methods to calculate PET provides similar results when a drought index, such as the PDSI, is calculated.

e. Point-by-point regression method

Simple correlation analysis between the tree-ring data and different seasonal combinations of SPEI identified June–August SPEI, calculated over a 3-month time scale, as the best target season for a hydroclimatic reconstruction over the study region. A point-by-point regression approach (PPR; Cook et al. 1999, 2004) was used to reconstruct the SPEI field from the tree-ring data. PPR is a form of a multiple linear regression technique in which the predictors are orthogonal principal components of the tree-ring data and the predictand is a field of climate variables. Most of the previous PPR based hydroclimatic reconstructions (e.g., Cook et al. 1999, 2004, 2010; Touchan et al. 2011) have used a search radius (SR) method to select tree-ring data for each gridpoint reconstruction from a network of tree-ring sites. A circle with a fixed radius is centered over each climate grid point. Chronologies from sites that fall within this circle are selected as candidate tree-ring predictors of drought at that specific point. The premise behind the SR method is that climate is more or less homogeneous in space. However, a complex topographical landscape may cause a marked climatic gradient throughout a region, especially a high spatial heterogeneity in soil moisture distribution, thereby causing spatially variable patterns in the tree-ring data response to climate. Fang et al. (2011) introduced a "search spatial correlation contour" (CC) method to select tree-ring chronologies for a PPR reconstruction of precipitation in northwest China, a region of variable climate and complex topographical landscape. The idea behind this method is to use correlation maps to determine the similarity of climate between the target grid point for reconstruction and the surrounding areas, and then to select the tree-ring chronologies located in areas with comparable climate regime to the target climate grid point. In this study both the SR and CC methods were tested in order to identify the most appropriate approach for a PPR-based moisture reconstruction over the Fennoscandian region.

It is not uncommon for tree-ring data to reflect a mix of current and previous years' environmental conditions (Fritts 2001). Hence, in order to correct for the difference in the short-lag persistence in tree-ring and climate data, all precipitation-sensitive tree-ring chronologies

(selected through prescreening 1) and observed SPEI data were autoregressive (AR) prewhitened over the 1901–76 common period, using a low-order AR model (maximum order = 3; the order of the model was determined using the Akaike information criterion; Akaike 1974). The prewhitening procedure reduced the climate and tree-data overlap to the 1904–76 period. Spatial CC maps were calculated between SPEI and tree-ring data over the 1904–76 period. Previous studies have used a dynamic SR and CC (Cook et al. 1999; Fang et al. 2011) when locating tree-ring chronologies for each gridpoint reconstruction, so that if no (or too few) chronologies are located around each grid, the CC and SR will expand until a prescribed number of chronologies have been found. This approach could be preferable if the tree-ring network is patchy, implying that some areas of the grid will require smaller SR/CC than other areas to locate the tree-ring data. The PPR approach in the current study was slightly different from the previous ones in that it used a fixed SR and CC. This option was chosen because 1) there is relatively dense and even tree-ring network over the Fennoscandian region and 2) a consistency in the SR and CC makes a comparison among the gridpoint reconstructions more straightforward. Candidate tree-ring chronologies located within a defined CC and SR around each specific grid point were retained for an additional screening prior to the regression analysis (referred to as screening 2). The purpose of this screening was to eliminate tree-ring chronologies insensitive to SPEI at each specific grid point. It was accomplished by correlating prewhitened tree-ring chronologies with prewhitened SPEI data over the calibration period. Only the response of tree-ring data to SPEI in the current year (t) was considered in the screening, and a two-tailed screening probability of $\alpha = 0.05$ was used as the selection criterion. Principal component analysis (PCA) was performed on the retained chronologies whereby orthogonal eigenvectors were generated. The lower-order tree-ring eigenvalues (>1.0), accounting for most of the common variance, were entered into a multivariate stepwise linear regression based on the R^2 statistic. The quality and temporal stability of the regression models was assessed through a split-sample method (Gordon 1982) that divided the period of climate and tree data overlap (1904–76) into two subsets of roughly equal length (1904–40 and 1941–76). Calibration and verification statistics were calculated for the first and the second half of the base period, respectively. The calibration and verification periods were then exchanged and the process repeated. The final models were derived over the full 1904–76 period. The validation of the regression models was performed by means of the calibration and

verification R^2, the reduction of error (RE) and co-efficient of efficiency (CE) statistics (National Research Council 2006). Only grid points that produced signifi-cant calibration regression models (p value of the F statistic < 0.05) and had both a CE and RE values ex-ceeding a zero threshold value were used to produce the final full-period calibration models.

f. Selection of the search radius and correlation contour

To determine the ideal SR and CC for a SPEI re-construction over the Fennsocandian region, multiple PPR runs were conducted in which the SR and CC varied over a wide range of values. The similarity be-tween all gridpoint reconstructions, produced by the full-period calibration models for each SR and CC run respectively, were assessed through correlation and plotted as a function of distance between the grid points. The same procedure was done for observed SPEI data from overlapping grids. The SR and CC that were able to capture the spatial decorrelation pattern of observed SPEI were selected for reconstructing drought across Fennoscandia.

g. Spatial comparison of observed and reconstructed SPEI

Three different metrics were used to assess the agreement between yearly fields of reconstructed and observed SPEI data: 1) mean field comparison of ob-served and reconstructed SPEI over time, 2) Pearson correlation coefficient, and 3) map congruence. The former was obtained by simply averaging the recon-structed field for every year, and comparing it with the yearly mean of observed SPEI data from overlapping grid points. The difference between Pearson product moment correlation and the congruence coefficient is that the former provides a measure of how well the relative spatial patterns of two climate fields covary, while the latter is a measure of the similarity in the ab-solute spatial patterns between the two fields. The only difference in the computation of these two metrics is that, unlike the calculation of the correlation co-efficients, the computation of the congruence co-efficients does not require the means of the reconstructed and observed climate fields to be removed [detailed descriptions on how to calculate the co-efficients can be found in Cook et al. (1999)]. Correla-tion and congruence coefficients were calculated between each annual pair of reconstructed and observed SPEI field. The reconstructed SPEI field was divided into three subregions: southern (lat. $< 60.5°$; 159 grid points), central ($60.5° \leq$ lat. $< 66.0°$; 371 grid points) and northern (lat. $> 66.0°$; 318 grid points) regions. The

spatial extent of the southern subregion was set to in-clude all the newly sampled xeric site chronologies, and the other two regions were arbitrarily set to roughly equal size. Mean field, map correlations, and congru-ences were calculated for the entire reconstructed re-gion, and for each subregion.

3. Results

a. SPEI reconstruction

A network of 125 precipitation-sensitive site chro-nologies, out of a total number of 179 screened chro-nologies, was preselected (screening 1) for the PPR run. The network comprises 85 TRW chronologies, 29 MXD chronologies, and six $\delta^{13}C$ and four $\delta^{18}O$ chronologies (Fig. 2). (Chronology information is available online as supplementary material, at http://dx.doi.org/10.1175/ JCLI-D-13-00734.s1).

Figure 3 compares spatial decorrelation patterns, av-eraged over 50-km blocks, of observed and re-constructed SPEI fields resulting from multiple PPR test runs in which the CC and SR have been varied over a range of values. A 0.76 CC and a 210-km SR produce spatial coherence patterns that most closely resemble the observed [lowest mean absolute error (MAE)]. Correlation magnitudes are slightly overestimated for the reconstructed datasets compared to the observed one for distances up to approximately 700 km, and un-derestimated for the SR reconstruction at distances ex-ceeding 1400 km. Reconstructions that are produced using search radii and correlation contours above (be-low) the $r = 0.76$ and 210-km threshold values exhibit correlograms with systematically larger (smaller) co-herence over distance than the correlogram developed from the observed SPEI data. This overestimation (underestimation) of observed spatial autocorrelation pattern is most likely due to a high (small) number of tree-ring predictors that are shared between each grid-point reconstruction. Consequently, the results indicate that a CC of 0.76 and an SR of 210 km are optimal, producing reconstructions that capture the true spatial autocorrelation patterns of droughts and pluvials in the Fennoscandian region. The following results are based on these search criteria.

b. Calibration and verification results

Contour maps of split-sample calibration and verifi-cation statistics for the SR and CC methods are shown in Fig. 4. The PPR runs using a 210-km SR and a 0.76 CC produces rather similar patterns in its overall re-construction skill. Significant calibration models are obtained for about 75% of the SPEI grid net for both early and late calibration periods. The rest of the grid
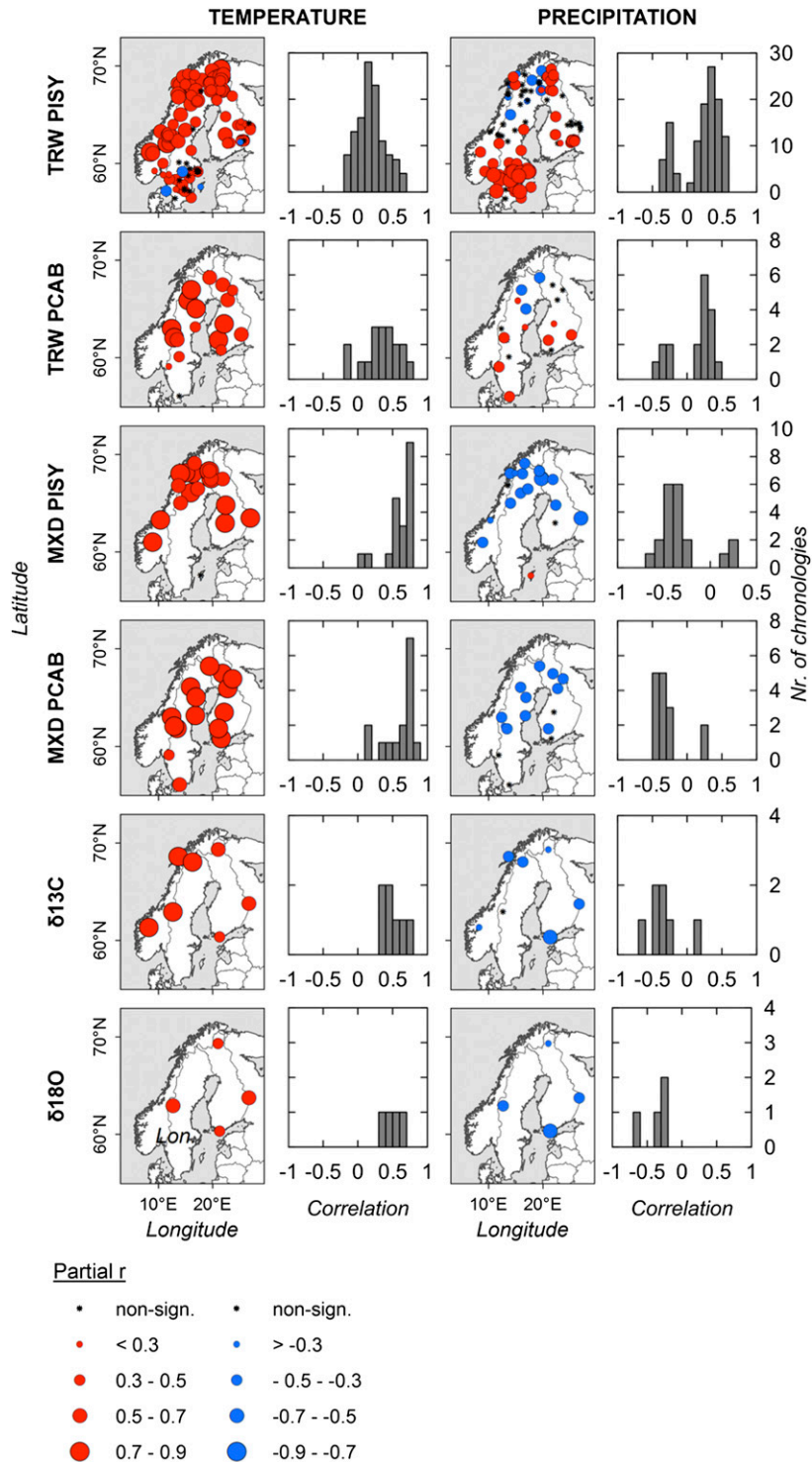
FIG. 2. Partial correlation between various tree-ring proxies and best-fit temperature and precipitation data (=target season). The proxy data are tree-ring width (TRW), maximum density (MXD), and stable carbon (δ^{13}C) and oxygen (δ^{18}O) isotopes from Scots pine (PISY) and Norway spruce (PCAB). The climate data were divided into individual months as well as all possible seasonal combinations over a 6-month window, extending from April to September of the current year. The month and season giving the highest correlation coefficient are presented here. Only the magnitudes of the correlation are indicated, and not the length and timing of the target season. Correlation analysis is based on first differences over the 1902–76 common period; $p < 0.05$ for significant coefficients. Climate data are obtained from the CRU TS3.0 dataset.
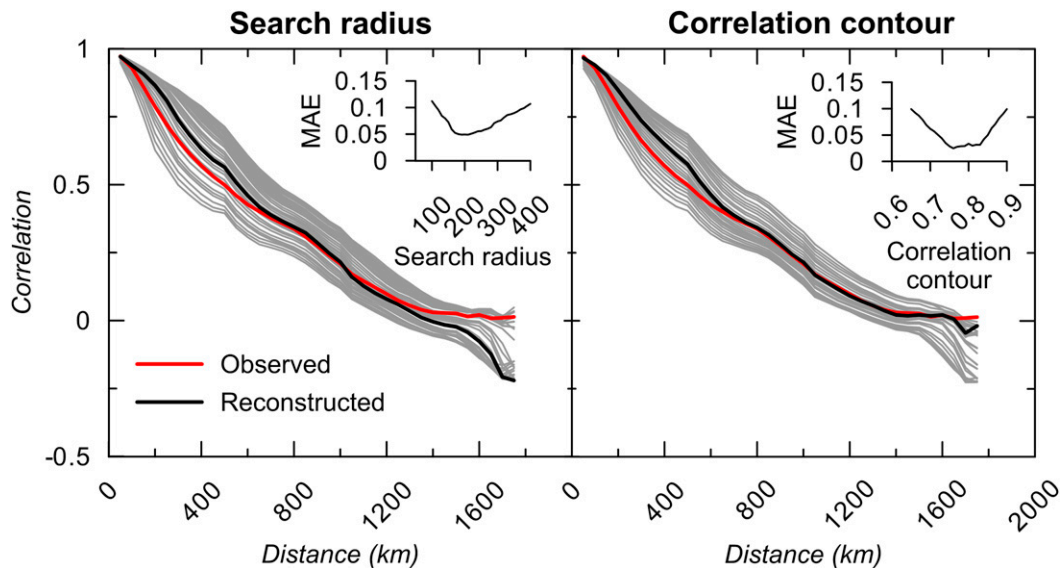
FIG. 3. Correlation between time series from the gridded SPEI field, as a function of distance between the grid points. The correlation has been calculated for observed (red lines) and reconstructed (black and gray lines) data, and averaged over 50-km intervals. Gray lines are correlation curves obtained from PPR runs where the SR has varied from 100 to 400 km and the CC from 0.65 to 0.90. Mean absolute error (MAE) shows how closely the correlation curve of the reconstructed fields follows the observed one. Black lines are the correlation curve for the lowest MAE. All the correlation curves, regardless of the method used, are based on exactly the same grid points (number of grid points = 580). The full-period calibration model (1904–76) has been used to reconstruct the SPEI, for grid points that were retained after the split-sample verification and calibration procedure.

points fail to reconstruct either because no chronologies are located within the SR/CC, or because the gridpoint regression model fail to pass the significance testing (F value > 0.05). There is a considerable regional variability in the calibration/verification statistics. The best calibration areas are located in south-central and northern Sweden, and southeastern and southwestern Finland, while the weakest calibration areas include Norway and western Sweden. Slightly better calibration and verification results are obtained for the early subperiod (1904–40) compared to the later one (1941–76). Median calibration and verification, R^2, and CE are approximately 40%, 35%, and 0.25, respectively. Roughly 10% and 15% of the reconstructed grid points, produced by the CC and SR methods respectively, fail to verify in the validation periods (CE and RE < 0). The weakest validation areas include the Norwegian coast, eastern Finland, and the southernmost and northernmost parts of the target domain.

Full period (1904–76) calibration was performed only on those grid points that were successfully calibrated and validated in the early and late subperiods. That included 827 grid points for the SR run and 848 grid points for CC run, predominantly located over Sweden and Finland. The contour method calibration R^2 values range between 13% and 65%, with a median value of

37% (Fig. 5a). The regression models obtained by the SR method explain between 13% and 60% of the SPEI variance, with a median of 36% (map not shown). Both methods produce coherent areas with the highest R^2 values along the southwestern coast of Finland, and in the interior of the northernmost parts of the target domain. The regression models produced by the radius method explains slightly more of the variance in observed SPEI over Sweden and Norway compared to the contour method, while the latter performs better over Finland and the northern portion of the target domain (Fig. 5b). Topography causes the spatial precipitation distribution to be rather heterogeneous over Norway and western part of Sweden (Fig. 1b). A CC of $r = 0.76$ thus produces relatively narrow contour areas over the region. Hence, in contrast to the SR, the CC method fails to include some of the tree-ring data that may have an actual relationship with drought at each specific grid point. On the other hand, the method is shown to be superior to the SR over northern and central parts of Finland, where the tree-ring network is less dense and where drought is more homogenous in space (Fig. 5c). Consequently, this affects the number of chronologies that passed the PPR screening, and, as seen in Fig. 5b, results in additional reconstruction skill. As the reconstructed SPEI fields produced by the SR and CC
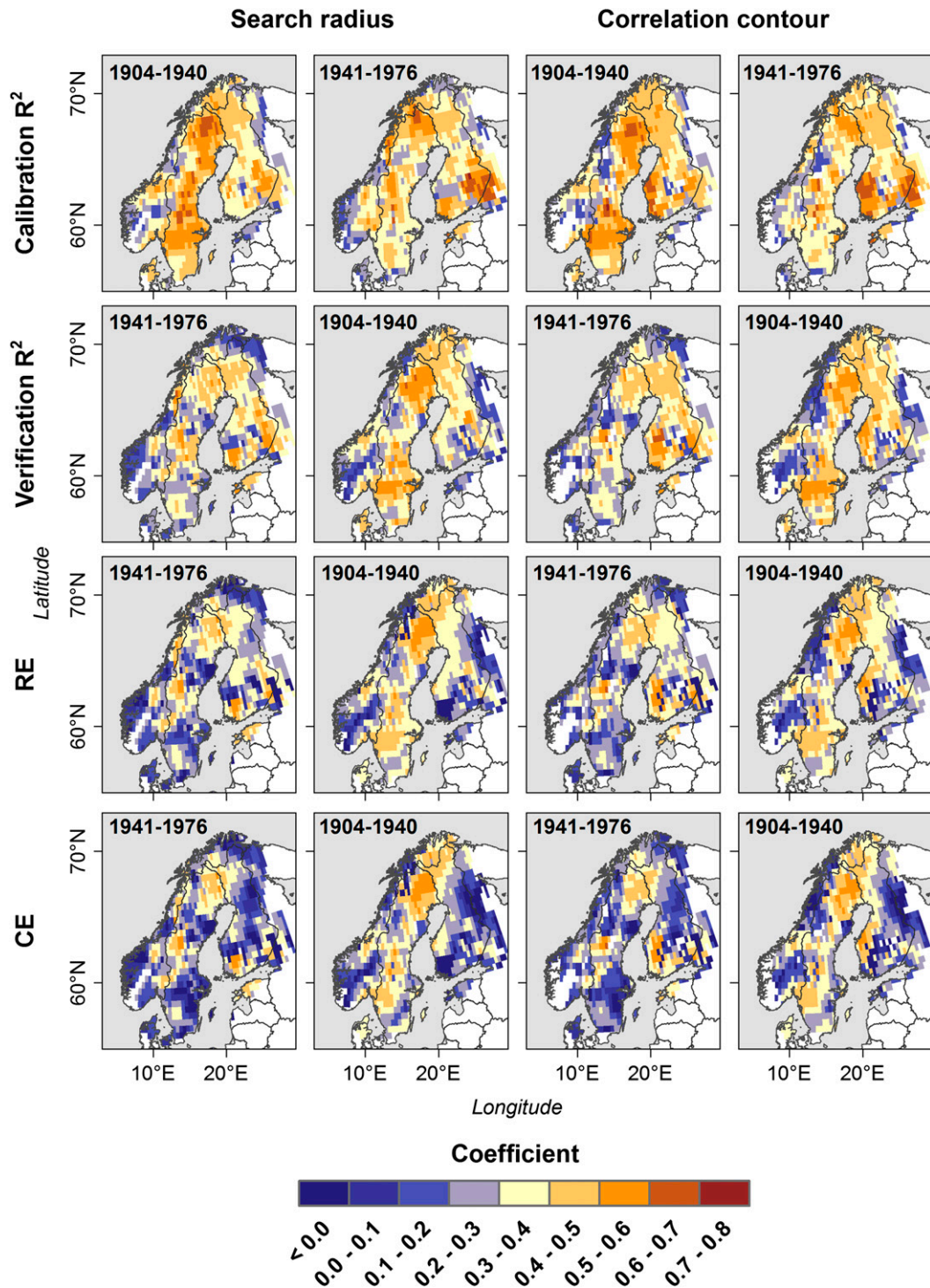
FIG. 4. Maps of calibration and verification statistics for the two subperiods (1904–40 and 1941–76) used in the split-sample calibration/verification procedure. Two different methods were used in the PPR approach to locate chronologies around each specific grid point: the search radius and correlation contour methods.
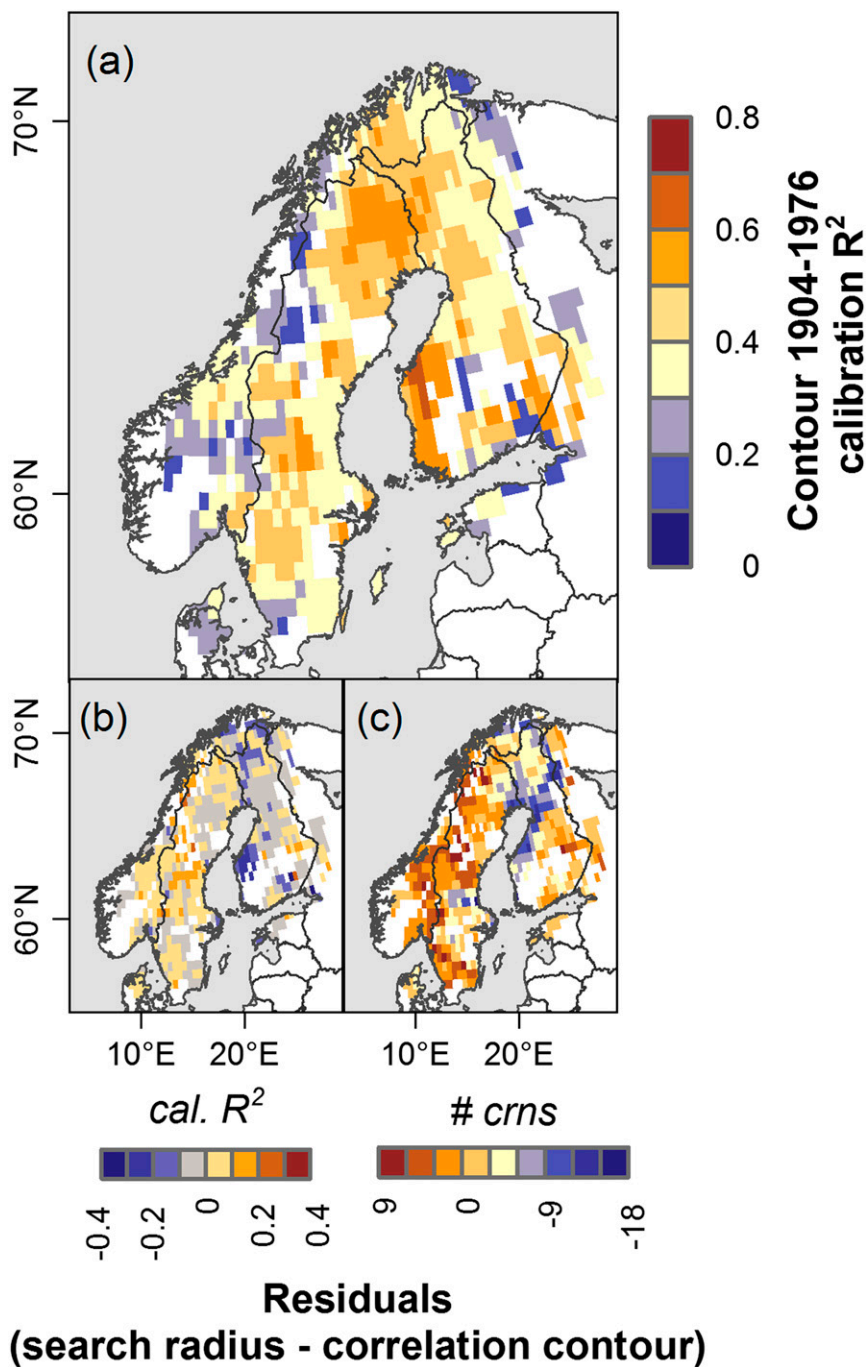
FIG. 5. (a) Full-period (1904–76) calibration R^2 using the CC method. Only grid points that have passed the split-sample calibration and verification procedure have been retained for the final full-period calibration. (b) The difference between full-period calibration R^2 values obtained by the SR method and the CC method. (c) The difference in the number of chronologies located for each gridpoint reconstruction using the two methods.
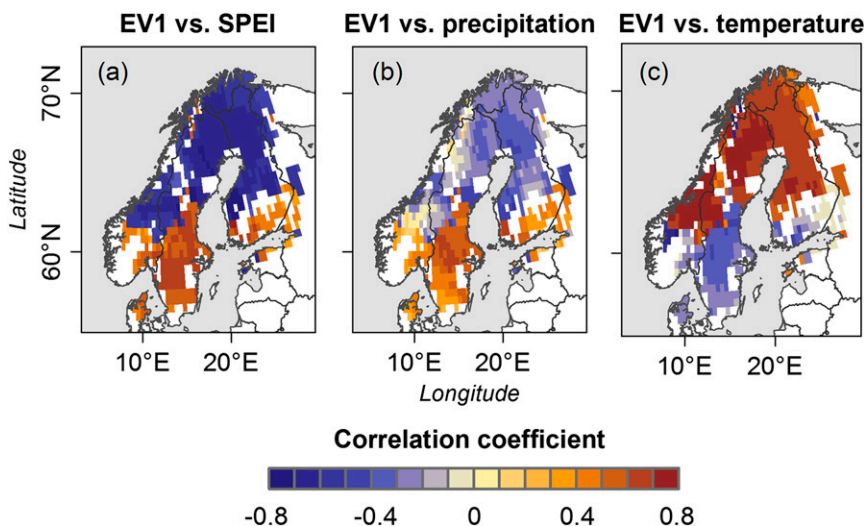
FIG. 6. Correlation between the scores of the first principal component from the tree-ring data and gridded (a) June–August SPEI, (b) April–August precipitation, and (c) April–August temperature over the 1904–76 time period. Temperature and precipitation data are from the CRU TS3.0 dataset.

methods in general show similar patterns, only results produced by the CC method will be discussed hereafter.

c. Climate response

The scores of the first principal component of the tree-ring data (EV1) at each grid point, produced by the PPR technique, is in general the component that has the strongest relationship with SPEI, thus having the highest contribution to the predictive power of each gridpoint reconstruction model. Correlation between EV1 for each reconstructed grid point and SPEI clearly identifies a northern and a southern subregion (Fig. 6a). The dominant mode of variability of the tree-ring data retained for the hydroclimate reconstruction is positively related to SPEI in the southern region (median correlation $r_m = 0.57$), implying that a majority of the tree-ring data is responding positively to increased moisture availability in this region. The opposite is true for the northern subregion, where there is a negative relationship between tree-ring data and increased wetness ($r_m = -0.60$). A similar pattern is found when comparing EV1 to gridded precipitation and temperature data (Figs. 6b,c). The strongest association between EV1 and precipitation is obtained for the southern region, where the relationship is positive (median $r = 0.46$). A negative, and weaker, association is found for the northern region ($r_m = -0.28$). The temperature response shows an inverse pattern, characterized by a strong and positive response of tree-ring data to temperatures in the northern part of the region ($r_m = 0.67$), and a much weaker negative response in the southern part of the

target domain ($r_m = -0.28$). These relationships broadly correspond to the pattern in the response of tree-ring data to temperature and precipitation identified through prescreening of the tree-ring archive (screening 1; Fig. 2).

d. Spatial comparison of observed and reconstructed SPEI

Figure 7 shows yearly means of observed and reconstructed SPEI fields, averaged over the entire reconstructed region and over three subregions. Correlations between observed and reconstructed mean series are highly significant ($p < 0.01$), demonstrating that the mean SPEI field is well predicted by the tree-ring data over the 1904–76 period. Correlation and congruence coefficients for the entire region and three subregions are presented in Fig. 8. Average correlation and congruence coefficients over the full 1904–76 period, obtained for the entire reconstructed region, are 0.40 and 0.52, respectively; the highest single-year values are 0.91 (year 1923) and 0.82 (year 1960), respectively. Overall, both correlation and congruence coefficients show high interannual variability. The latter is even displaying negative values for occasional years (e.g., year 1919 calculated for the entire region). Especially the northern region shows a high spread in both coefficients, which frequently take on negative values, whereas reconstructions over the central region show an overall high spatial performance.

Figure 9 compares annual contour maps of observed and reconstructed SPEI for selected years, characterized
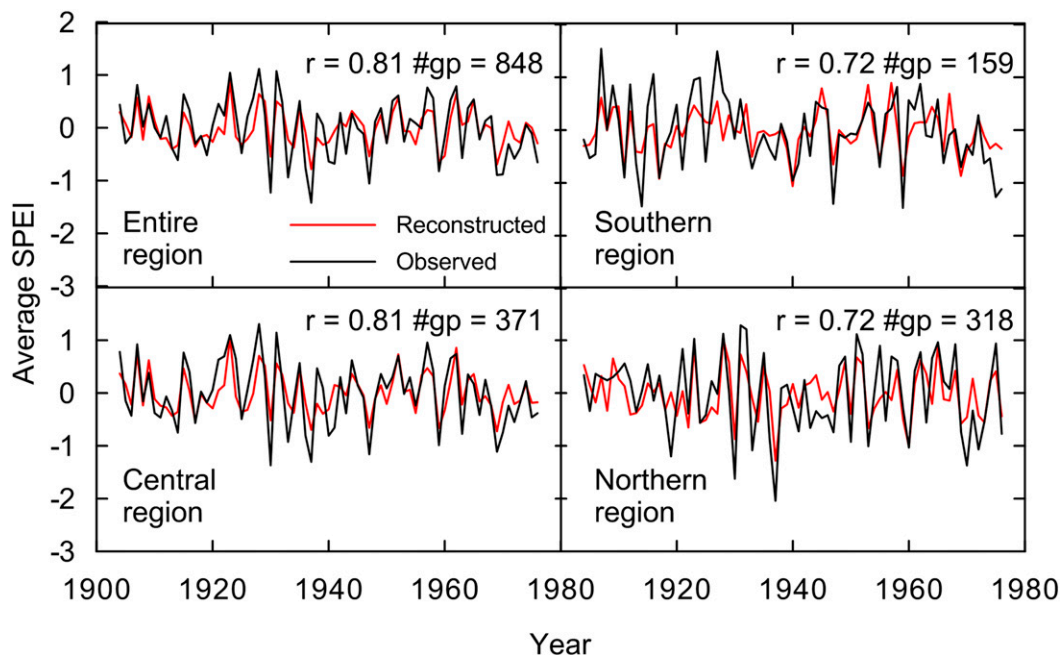
FIG. 7. SPEI field averaged over each year over the whole reconstructed region, and the southern, central, and northern subregions. Mean values of the observed SPEI data comes from overlapping grid points.

by high congruence and correlation coefficients. The reconstructed fields are able to capture the general spatial features of observed moisture distribution. Distinctive subregional drought and pluvial cells (e.g., years 1910 and 1953), as well as more or less regional-wide episodes (years 1923 and 1937), are replicated by the tree-ring reconstructions. A few anomalies, predominantly located over the northern portion of the target domain, are underestimated (e.g., years 1910, 1937, and 1968). Annual contour maps of observed and reconstructed SPEI for poorly modeled years are shown in Fig. 10. It is evident that the reconstruction fails to adequately estimate the spatial pattern and the magnitude of observed data these years, especially the smaller-scale SPEI anomalies.

Individual years were classified as being either dry or pluvial. The classification was based on observed SPEI data, over the 1904–76 period, from grid points that had successfully been used in the reconstruction. A year was classified as being dry (pluvial) if SPEI was below (above) average for more than half of the grid net. The intensity of the anomaly was assessed by quantifying the size of the area (number of grid points) covered by observed SPEI values below −1 (for dry years) or above 1 (for pluvial years). Figure 11 shows the size of the area (denoted as % of the total 848 grid points) versus the congruence coefficient of each individual year (the years are marked out in Fig. 8). There is

a clear positive relationship between the spatial extension of the anomaly of each year and the ability of the reconstructed grid to capture the magnitude of the anomaly in observed SPEI data.

4. Discussion

This study is the first to assess the potential of applying a dendroclimatological multiproxy approach to reconstruct past spatial patterns of hydroclimatic variability in the Fennoscandian region, using a point-by-point multiple nested regression approach (Cook et al. 1999). We tested both a fixed SR and a CC method to locate candidate tree-ring chronologies for each gridpoint reconstruction. As confirmed by several metrics of reconstruction fidelity, there are some regional differences between the reconstructions produced by both methods. These mainly arise from the spatial properties of the target climate field. In contrast to what can be expected, the SR is superior to the CC method in mountainous western Fennoscandia, whereas the opposite is true over the lowlands in the eastern-northeastern parts of the target domain. Our results suggests that even though a CC of 0.76 (SR of 210 km) might produce on average the best reconstructions across the grid and capture the general spatial autocorrelation patterns of observed SPEI, it is not screening large enough areas
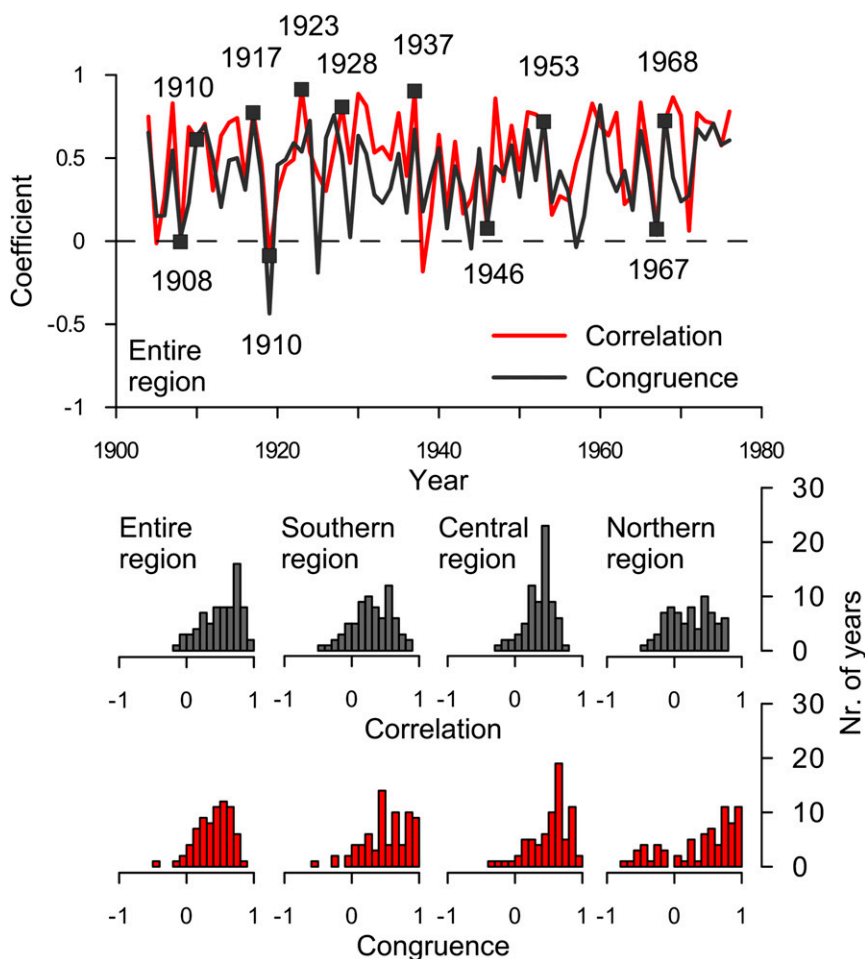
FIG. 8. Correlation and congruence coefficients, comparing each annual map pairs of observed and reconstructed SPEI. The reconstruction is obtained from the full 1904–76 calibration model, using the CC method. The coefficients are calculated for the full reconstructed region, and the southern, central, and northern subregions. The squares in the upper plot mark out the years that are illustrated in Figs. 9 and 10.

over topographically variable regions to include all of the "true" tree-ring predictors of SPEI. This result points toward the difficulty of finding a single optimal SR/CC combination for a topographically and climatologically diverse area. To estimate the best possible reconstruction of SPEI at each location would require individual modeling of each grid point in the target field, which is a very time-consuming and tedious option. An SR of 210 km corresponds roughly to the correlation decay distance (defined as the distance where the correlation between one station and all other stations decays below $1/e$) determined by Hofstra and New (2009) based on independent evaluation of summer precipitation data over northern Europe. These results suggest a convective influence on the summertime rainfall distribution in the region,

which is also captured by the tree-ring archive, rather than frontal conditions that generally have a larger spatial scale.

The calibration and verification statistics describing the accuracy of our reconstruction in a temporal sense (i.e., calibration/verification R^2, RE, and CE) are remarkably high for a dendroclimatic reconstruction, especially when considering the cool and moist climate of the study region [cf. hydroclimatic reconstructions in Linderholm et al. (2010)]. To this date, few attempts have been made to provide moisture reconstructions for the Fennoscandian region. The work that has been done has focused on reconstructing the temporal variability of hydroclimate, omitting its spatial component. The majority of the individual gridpoint reconstructions provided in this study have shown considerably higher
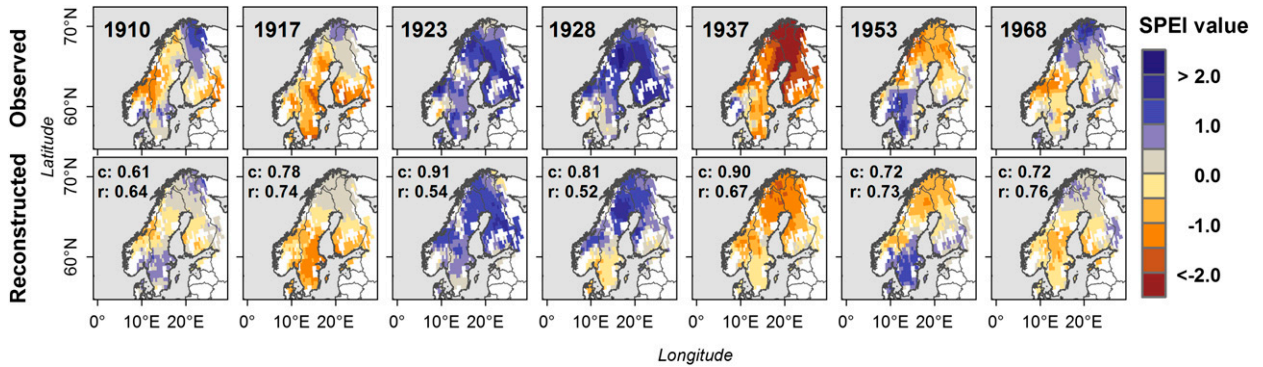
FIG. 9. Maps of reconstructed and observed SPEI for selected years, characterized by high congruence and correlation coefficients (obtained for the entire reconstructed region).

temporal accuracy than the earlier hydroclimatic reconstructions from the region (e.g., Helama and Lindholm 2003; Linderholm and Molin 2005; Jönsson and Nilsson 2009; Drobyshev et al. 2011; Seftigen et al. 2013). The successful application of tree-ring data from temperate and subarctic Fennoscandia in the current reconstructions is likely a product of the nature of SPEI. Tree-ring data from the region describe signals related to both temperature and precipitation, and a reconstruction of a drought index that combines both variables is thus likely to yield an overall better result than estimations of precipitation and temperatures separately, or estimations of a precipitation-based drought index such as SPI. In Fig. 12 a PPR-produced calibration R^2 map, over the target region where the SPEI target climate field has been replaced with SPI, is shown. The general ability of the tree-ring proxy data to reconstruct this precipitation-based drought index is indeed poorer than a temperature- and precipitation-based index such as the SPEI (median calibration

$R^2 = 18\%$; cf. Fig. 5a). The performance peaks in the southern part of the domain, whereas the calibration skill in the north, where the tree-ring data are mainly temperature dependent, is in general quite poor.

While each individual gridpoint reconstruction is reasonably accurate, it is not a guarantee that the reconstructed fields will be valid in a spatial sense. Our results, however, clearly demonstrate that the *mean* fields of observed SPEI are estimated exceptionally well over the twentieth century by the reconstruction. Moreover, the mean correlation and congruence coefficients over the full calibration period are only marginally lower than those identified in NADA (Cook et al. 1999), comparing observed and estimated PDSI over the entire continental United States. These values support a long-term overall spatial representativeness of the reconstructed field. The ability to replicate annual spatial patterns is, however, not consistent throughout time, but shows variability on an interannual basis. There is no doubt that those years that performs well are
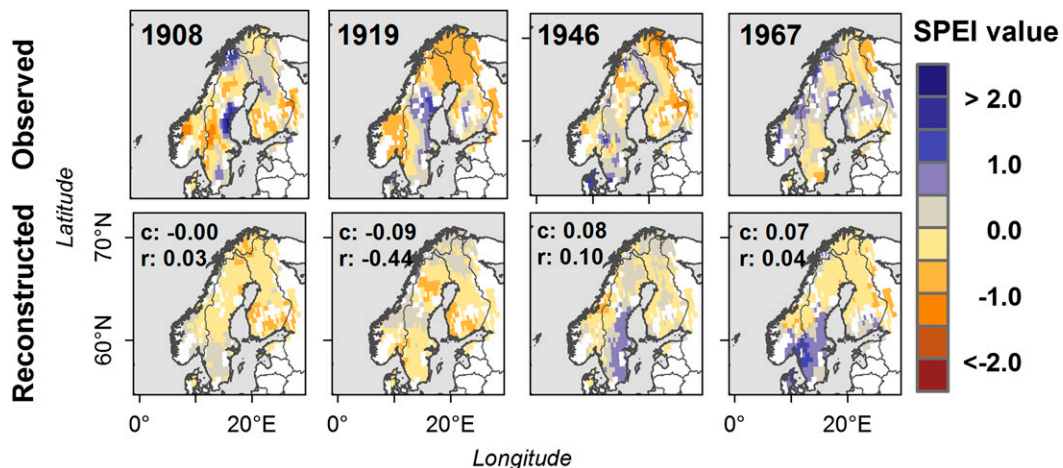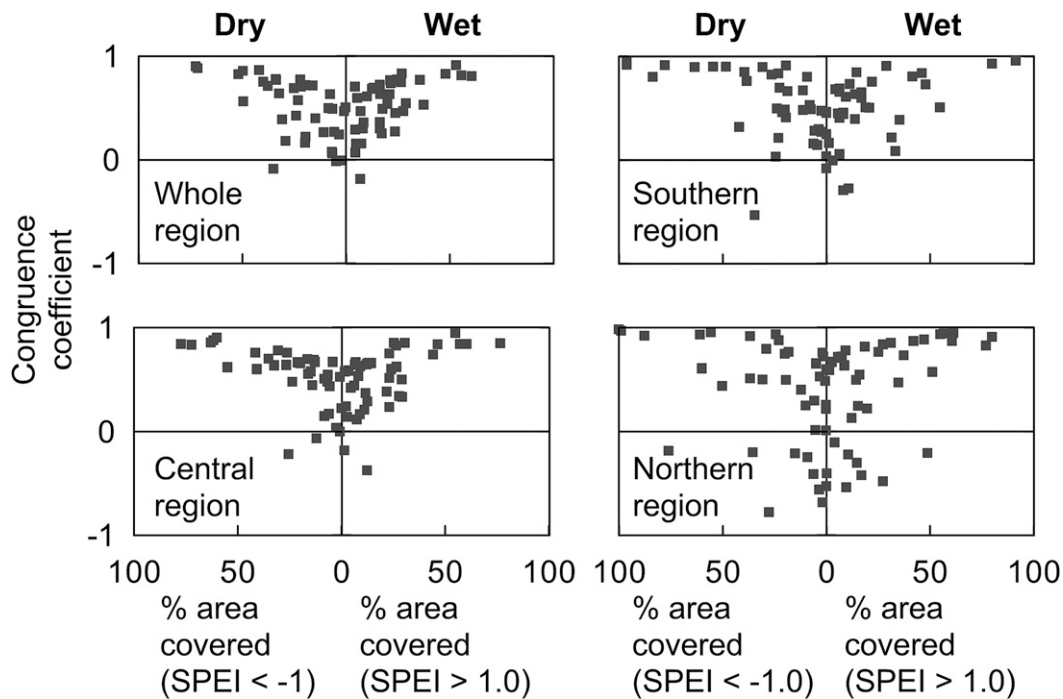

FIG. 10. As in Fig. 9, but for poorly modeled years.

FIG. 11. Congruence coefficient, obtained separately for dry (SPEI below average for >50% of the area) and wet years (SPEI above average for >50% of the area), displayed as a function of percent area covered by the extreme (here defined as SPEI < −1 or > 1).

able to capture most of the regional-wide anomalies as well as finer-scale climatology. Annual patterns of poorly modeled years are either overestimating (or underestimating) the magnitude of the anomaly, or are including grid points that are not capable of capturing the relative spatial pattern of observed SPEI. Although we can only speculate as to the drivers behind poorly modeled years, our results suggest that the tree-ring estimates are failing to capture the finescale heterogeneity of SPEI over certain years, rather than its broad-scale spatial structure. This might be 1) because the tree-ring network is not dense enough to capture all small-scale climate anomalies or 2) because of the strong geographical pattern in the climate response of the tree-ring data used for the reconstruction. Anomalous rainfall patterns are the main drivers behind local anomalies in SPEI. This is because temperatures exhibit a higher spatial autocorrelation pattern than precipitation (Jones et al. 1997; Hofstra and New 2009). The tree-ring data used in the SPEI reconstruction are sensitive to different aspects of climate; a temperature signal dominates the tree-ring data in the north and a precipitation signal in the southern part of the target domain. This suggests that tree rings from the northern region might perform well in reconstructing temperature-induced drought stress, but on the other hand may be insufficient in

reconstructing smaller-scale drought patterns caused by a precipitation shortage. An overall low spatial performance of the reconstruction over the northernmost part of the domain, as described by the congruence and correlation coefficients, supports this idea. Furthermore, precipitation-induced droughts are probably best captured by the reconstruction in the southern portion of the target field, where the tree-ring data are related to SPEI mainly through their relation to precipitation. Hence, an overall high spatial performance of the reconstructed field over the central region can be explained by the fact that its pool of candidate tree-ring predictors both includes data from the north and from the south, contributing both a temperature and a precipitation flavor to the reconstruction.

The work outlined herein is the first step toward an improved understanding of past spatiotemporal drought variability in Fennoscandia. Although the study focuses on the twentieth century only, the tree-ring archive that is used herein extends well beyond the instrumental era. The bulk of the longest continuous tree-ring records, covering in several cases the full length of the past millennia, are presently predominantly located in the northern parts of the target domain. The southern portions of the network, on the other hand, rarely extend beyond the time span covered by the living trees
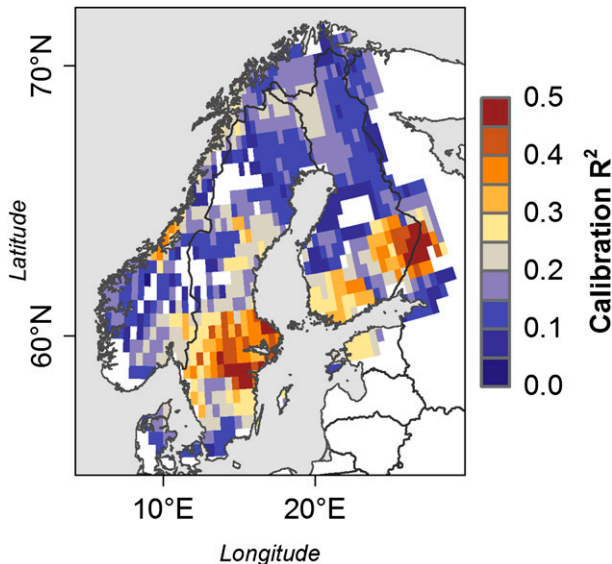
FIG. 12. Calibration R^2 map, using a 3-month June–August SPI as the target climate field. The calibration has been performed over the 1904–76 interval, using an SR of 210 km to locate the tree-ring data.

($\sim$250–350 yr). Hence, an important future direction for Fennoscandian tree-ring-based hydroclimate field reconstructions is an extension of the temporal coverage of the moisture-sensitive tree-ring network, to enable assessments of hydroclimate over longer time scales. This could potentially be done by combining living tree-ring series with relict wood extracted from small lakes throughout the region. This has previously been done by Helama and Lindholm (2003) and Helama et al. (2009), who were able to push the tree-ring archive in southern Finland beyond the past millennia by using tree logs preserved in lacustrine sediments. Ongoing collections throughout the target domain, especially in areas that are now weakly modeled, should also continuously improve the capability to study spatial patterns of droughts and pluvials in Fennoscandia.

5. Concluding remarks

This study is the first attempt to derive tree-ring-based field reconstructions of twentieth-century moisture variability for the Fennoscandian region. The reconstructions show a remarkably high accuracy in a temporal sense, especially considering the climatological settings of the region. The overall spatial performance of the reconstructed field is generally quite good. Our validation results suggest that the reconstruction has the greatest spatial skill in central and southern Fennoscandia. A relatively low reconstruction skill, by contrast, is found in the northern part of the target region. We caution that

a complicating factor for a tree-ring-based spatial SPEI reconstruction in the Fennoscandian region might be a geographically varying response of tree-ring data to temperature versus precipitation. The severity of this factor has not been conclusively investigated, and needs further attention.

This exploratory study has demonstrated that a point-by-point regression method can be applied to dendrochronological data to explore past moisture conditions in Fennoscandia. The future direction in the field will be to provide a long-term context for the Fennoscandian hydroclimate by producing reconstructions extending beyond the observational record.

REFERENCES

Akaike, H., 1974: A new look at the statistical model identification. *IEEE Trans. Autom. Control,* **19,** 716–723, doi:10.1109/TAC.1974.1100705.

Alcamo, J., M. Flörke, and M. Märker, 2007: Future long-term changes in global water resources driven by socio-economic and climatic changes. *Hydrol. Sci.,* **52,** 247–275, doi:10.1623/hysj.52.2.247.

Allen, R. G., M. Smith, A. Perrier, and L. S. Pereira, 1994a: An update for the definition of reference evapotranspiration. *ICID Bulletin,* No. 43, International Commission on Irrigation and Drainage, New Delhi, India, 1–34.

——, ——, ——, and ——, 1994b: An update for the calculation of reference evapotranspiration. *ICID Bulletin,* No. 43, International Commission on Irrigation and Drainage, New Delhi, India, 35–92.

Blasing, T. J., and D. Duvick, 1984: Reconstruction of precipitation history in North American corn belt using tree rings. *Nature,* **307,** 143–145, doi:10.1038/307143a0.

Boorman, D. B., 2003: LOIS in-stream water quality modelling. Part 2. Results and scenarios. *Sci. Total Environ.,* **314–316,** 397–409, doi:10.1016/S0048-9697(03)00065-2.

Busuioc, A., D. Chen, and C. Hellström, 2001: Temporal and spatial variability of precipitation in Sweden and its link with the large-scale atmospheric circulation. *Tellus,* **53A,** 348–367, doi:10.1034/j.1600-0870.2001.01152.x.

Chang, T. J., and X. A. Cleopa, 1991: A proposed method for drought monitoring. *J. Amer. Water Resour. Assoc.,* **27,** 275–281, doi:10.1111/j.1752-1688.1991.tb03132.x.

Cook, E. R., and G. C. Jacoby, 1977: Tree-ring-drought relationships in the Hudson Valley, New York. *Science,* **198,** 399–401, doi:10.1126/science.198.4315.399.

——, and K. Peters, 1981: The smoothing spline: A new approach to standardizing forest interior tree-ring width series for dendroclimatic studies. *Tree-Ring Bull.,* **41,** 45–53.

——, M. A. Kablack, and G. C. Jacoby, 1988: The 1986 drought in the southeastern United States: How rare an event was it? *J. Geophys. Res.,* **93,** 14 257–14 260, doi:10.1029/JD093iD11p14257.

——, D. W. Stahle, and M. K. Cleaveland, 1992: Dendroclimatic evidence from eastern North America. *Climate since 1500,* R. S. Bradley and P. D. Jones, Eds., Routledge, 331–348.

——, D. M. Meko, D. W. Stahle, and M. K. Cleaveland, 1996: Tree-ring reconstructions of past drought across the coterminous United States: Tests of a regression method and calibration/verification results. *Tree Rings, Environment and Humanity; Proceedings of the International Conference, Tucson, Arizona, 17–21 May 1994,* J. S. Dean, D. M. Meko, and T. W. Swetnam, Eds., Radiocarbon, Dept. of Geosciences, University of Tucson, 155–169.

——, ——, ——, and ——, 1999: Drought reconstructions for the continental United States. *J. Climate,* **12,** 1145–1162, doi:10.1175/1520-0442(1999)012<1145:DRFTCU>2.0.CO;2.

——, C. A. Woodhouse, C. M. Eakin, D. M. Meko, and D. W. Stahle, 2004: Long-term aridity changes in the western United States. *Science,* **306,** 1015–1018, doi:10.1126/science.1102586.

——, R. Seager, M. A. Cane, and D. W. Stahle, 2007: North American droughts: Reconstructions, causes and consequences. *Earth-Sci. Rev.,* **81,** 93–134, doi:10.1016/j.earscirev.2006.12.002.

——, K. J. Anchukaitis, B. M. Buckley, R. D. D'Arrigo, J. C. Jacoby, and W. E. Wright, 2010: Asian monsoon failure and megadrought during the last millennium. *Science,* **328,** 486–489, doi:10.1126/science.1185188.

Drobyshev, I., M. Niklasson, H. W. Linderholm, K. Seftigen, T. Hickler, and O. Eggertsson, 2011: Reconstruction of a regional drought index in southern Sweden since AD 1750. *Holocene,* **21,** 667–679, doi:10.1177/0959683610391312.

EEA, 2004: Impacts of Europe's changing climate: An indicator-based assessment. EEA Rep. 2/2004, European Environment Agency, 107 pp.

Eklund, B., 1954: Årsringsbreddens klimatiskt betingade variation hos tall och gran inom norra Sverige åren 1900–1944 (The climatically induced variation of tree-ring width for pine and spruce in northern Sweden during 1900–1944). *Medd. Statens Skogsforskningsinst.,* **44,** 150 pp.

Erlandsson, S., 1936: Dendrochronological studies. Stockholm's College Geochronological Institute Rep. 23, 116 pp.

Fang, K., X. Gou, F. Chen, E. Cook, J. Li, B. Buckley, and R. D'Arrigo, 2011: Large-scale precipitation variability over northwest China inferred from tree rings. *J. Climate,* **24,** 3457–3468, doi:10.1175/2011JCLI3911.1.

Ferrier, R., and A. Edwards, 2002: Sustainability of Scottish water quality in the early 21st century. *Sci. Total Environ.,* **294,** 57–71, doi:10.1016/S0048-9697(02)00052-9.

Fisher, A., 2000: Preliminary findings from the mid-Atlantic regional assessment. *Climate Res.,* **14,** 261–269, doi:10.3354/cr014261.

Fritts, H. C., 2001. *Tree Rings and Climate.* Blackburn Press, 584 pp.

Gagen, M., D. McCarroll, and J.-L. Edouard, 2004: The effect of site conditions on pine tree ring width, density and δ^{13}C series in a dry sub-alpine environment. *Arct. Antarct. Alp. Res.,* **36,** 166–171.

——, ——, and ——, 2006: Combining tree ring width, density and stable carbon isotope series to enhance the climate signal in tree-rings: An example from the French Alps. *Climatic Change,* **78,** 363–379, doi:10.1007/s10584-006-9097-3.

Gilvear, D., K. Heal, and A. Stephen, 2002: Hydrology and the ecological quality of Scottish river ecosystems. *Sci. Total Environ.,* **294,** 131–159, doi:10.1016/S0048-9697(02)00060-8.

Gordon, G., 1982. Verification of dendroclimatic reconstructions. *Climate from Tree Rings,* M. K. Hughes et al., Eds., Cambridge University Press, 58–61.

Grissino-Mayer, H. D., and H. C. Fritts, 1997: The International Tree-Ring Data Bank: An enhanced global database serving the global scientific community. *Holocene,* **7,** 235–238, doi:10.1177/095968369700700212.

Guttman, N. B., 1998: Comparing the Palmer Drought Index and the Standardized Precipitation Index. *J. Amer. Water Resour. Assoc.,* **34,** 113–121, doi:10.1111/j.1752-1688.1998.tb05964.x.

Hansen, J., R. Ruedy, M. Sato, and K. Lo, 2010: Global surface temperature change. *Rev. Geophys.,* **48,** RG4004, doi:10.1029/2010RG000345.

Harris, I., P. D. Jones, T. J. Osborn, and D. H. Lister, 2013: Updated high-resolution grids of monthly climatic observations—The CRU TS3.10 dataset. *Int. J. Climatol.,* **34,** 623–642, doi:10.1002/joc.3711.

Heim, R. R., 2002: A review of twentieth-century drought indices used in the United States. *Bull. Amer. Meteor. Soc.,* **83,** 1149–1165, doi:10.1175/1520-0477(2002)083<1149:AROTDI>2.3.CO;2.

Helama, S., and M. Lindholm, 2003: Droughts and rainfall in southeastern Finland since AD 874, inferred from Scots pine ring-widths. *Boreal Environ. Res.,* **8,** 171–183.

——, J. Merilainen, and H. Tuomenvirta, 2009: Multicentennial megadrought in northern Europe coincided with a global El Niño–Southern Oscillation drought pattern during the Medieval Climate Anomaly. *Geology,* **37,** 175–178, doi:10.1130/G25329A.1.

Herweijer, C., R. Seager, E. R. Cook, and J. Emile-Geay, 2007: North American droughts of the last millennium from a gridded network of tree-ring data. *J. Climate,* **20,** 1353–1376, doi:10.1175/JCLI4042.1.

Hofstra, N., and M. New, 2009: Spatial variability in correlation decay distance and influence on angular-distance weighting interpolation of daily precipitation over Europe. *Int. J. Climatol.,* **29,** 1872–1880, doi:10.1002/joc.1819.

IPCC, 2013: Summary for policymakers. *Climate Change 2013: The Physical Science Basis,* T. F. Stocker et al., Eds., Cambridge University Press, 1–29.

Jones, P. D., T. J. Osborn, and K. R. Briffa, 1997: Estimating sampling errors in large-scale temperature averages. *J. Climate,* **10,** 2548–2568, doi:10.1175/1520-0442(1997)010<2548:ESEILS>2.0.CO;2.

——, D. H. Lister, T. J. Osborn, C. Harpham, M. Salmon, and C. P. Morice, 2012: Hemispheric and large-scale land-surface air temperature variations: An extensive revision and an update to 2010. *J. Geophys. Res.,* **117,** D05127, doi:10.1029/2011JD017139.

Jönsson, K., and C. Nilsson, 2009: Scots pine (*Pinus sylvestris* L.) on shingle fields: A dendrochronologic reconstruction of early summer precipitation in mideast Sweden. *J. Climate,* **22,** 4710–4722, doi:10.1175/2009JCLI2401.1.

Lawrimore, J. H., M. J. Menne, B. E. Gleason, C. N. Williams, D. B. Wuertz, R. S. Vose, and J. Rennie, 2011: An overview of the Global Historical Climatology Network monthly mean temperature data set, version 3. *J. Geophys. Res.,* **116,** D19121, doi:10.1029/2011JD016187.

Levanič, T., I. Popa, S. Poljanšek, and C. Nechita, 2013: A 323-year long reconstruction of drought for SW Romania based on black pine (*Pinus nigra*) tree-ring widths. *Int. J. Biometeor.,* **57,** 703–714, doi:10.1007/s00484-012-0596-9.

Linderholm, H. W., and T. Molin, 2005: Early nineteenth century drought in east central Sweden inferred from dendrochronological and historical archives. *Climate Res.,* **29,** 63–72, doi:10.3354/cr029063.

——, M. Niklasson, and T. Molin, 2004: Summer moisture variability in east central Sweden since the mid-eighteenth century recorded in tree rings. *Geogr. Ann.,* **86,** 277–287, doi:10.1111/j.0435-3676.2004.00231.x.

——, J. A. Björklund, K. Seftigen, B. E. Gunnarson, H. Grudd, J.-H. Jeong, I. Drobyshev, and Y. Liu, 2010: Dendroclimatology in Fennoscandia—From past accomplishments to future potential. *Climate Past,* **6,** 93–114, doi:10.5194/cp-6-93-2010.

Lloyd-Hughes, B., and M. A. Saunders, 2002: A drought climatology for Europe. *Int. J. Climatol.,* **22,** 1571–1592, doi:10.1002/joc.846.

Mavromatis, T., 2007: Drought index evaluation for assessing future wheat production in Greece. *Int. J. Climatol.,* **27,** 911–924, doi:10.1002/joc.1444.

McCarroll, D., and Coauthors, 2003: Multiproxy dendroclimatology: A pilot study in northern Finland. *Holocene,* **13,** 829–838, doi:10.1191/0959683603hl668rp.

——, M. Tuovinen, R. Campbell, M. Gagen, H. Grudd, R. Jalkanen, N. J. Loader, and I. Robertson, 2011: A critical evaluation of multi-proxy dendroclimatology in northern Finland. *J. Quat. Sci.,* **26,** 7–14, doi:10.1002/jqs.1408.

——, and Coauthors, 2013: A 1200-year multiproxy record of tree growth and summer temperature at the northern pine forest limit of Europe. *Holocene,* **23,** 471–484, doi:10.1177/0959683612467483.

McKee, T. B. N., J. Doesken, and J. Kleist, 1993: The relationship of drought frequency and duration to time scales. *Eighth Conf. on Applied Climatology,* Anaheim, CA, Amer. Meteor. Soc., 179–184.

Meehl, G. A., J. M. Arblaster, and C. Tebaldi, 2005: Understanding future patterns of precipitation intensity in climate model simulations. *Geophys. Res. Lett.,* **32,** L18719, doi:10.1029/2005GL023680.

Meko, D. M., 1992: Dendroclimatic evidence from the Great Plains of the United States. *Climate since A.D. 1500,* R. S. Bradley and P. D. Jones, Eds., Routledge, 312–330.

——, R. Touchan, and K. J. Anchukaitis, 2011: Seascorr: A MATLAB program for identifying the seasonal climate signal in an annual tree-ring time series. *Comput. Geosci.,* **37,** 1234–1241, doi:10.1016/j.cageo.2011.01.013.

National Research Council, 2006: *Surface Temperature Reconstructions for the Last 2,000 Years.* National Academies Press, 196 pp.

Palmer, W. C., 1965: Meteorological droughts. U.S. Department of Commerce Weather Bureau Research Paper 45, 58 pp.

Percival, D. B., and W. L. B. Constantine, 2006: Exact simulation of Gaussian time series from nonparametric spectral estimates with application to bootstrapping. *Stat. Comput.,* **16,** 25–35, doi:10.1007/s11222-006-5198-0.

Rohde, R., and Coauthors, 2013: A new estimate of the average Earth surface land temperature spanning 1753 to 2011. *Geoinfor. Geostat. Overview,* **1** (1), doi:10.4172/2327-4581.1000101.

Rumsby, B. T., and M. G. Macklin, 1994: Channel and floodplain response to recent abrupt climate change: The Tyne Basin, northern England. *Earth Surf. Processes Landforms,* **19,** 499–515, doi:10.1002/esp.3290190603.

Seftigen, K., H. W. Linderholm, I. Drobyshev, and M. Niklasson, 2013: Reconstructed drought variability in east-central Sweden since the 1650s. *Int. J. Climatol.,* **33,** 2449–2458, doi:10.1002/joc.3592.

Smith, R. B., 1979: The influence of mountains on the atmosphere. *Advances in Geophysics,* Vol. 21, Academic Press, 87–230.

Soulsby, C., C. Gibbins, A. Wade, R. Smart, and R. Helliwell, 2002: Water quality in the Scottish uplands: A hydrological perspective on catchment hydrochemistry. *Sci. Total Environ.,* **294,** 73–94, doi:10.1016/S0048-9697(02)00057-8.

Stahle, D. W., M. K. Cleaveland, and J. G. Hehr, 1985: A 450-year drought reconstruction for Arkansas, United States. *Nature,* **316,** 530–532, doi:10.1038/316530a0.

——, ——, and ——, 1988: North Carolina climate changes from tree rings: A.D. 372 to 1985. *Science,* **240,** 1517–1519, doi:10.1126/science.240.4858.1517.

Stockton, C. W., and D. M. Meko, 1975: A long-term history of drought occurrence in western United States as inferred from tree rings. *Weatherwise,* **28,** 244–250, doi:10.1080/00431672.1975.9931775.

——, and ——, 1983: Drought recurrence in the Great Plains as reconstructed from long-term tree-ring records. *J. Climate Appl. Meteor.,* **22,** 17–29, doi:10.1175/1520-0450(1983)022<0017:DRITGP>2.0.CO;2.

Stokes, M. A., and T. L. Smiley, 1968: *An Introduction to Tree-Ring Dating.* University of Chicago Press, 73 pp.

Thornthwaite, C. W., 1948: An approach toward a rational classification of climate. *Geogr. Rev.,* **38,** 55–94, doi:10.2307/210739.

Touchan, R., G. Funkhouser, M. K. Hughes, and N. Erkan, 2005: Standardized precipitation index reconstructed from Turkish tree-ring widths. *Climatic Change,* **72,** 339–353, doi:10.1007/s10584-005-5358-9.

——, K. J. Anchukaitis, D. M. Meko, M. Sabir, S. Attalah, and A. Aloui, 2011: Spatiotemporal drought variability in northwestern Africa over the last nine centuries. *Climate Dyn.,* **37,** 237–253, doi:10.1007/s00382-010-0804-4.

Vicente-Serrano, S. M., S. Beguería, and J. I. López-Moreno, 2010: A multiscalar drought index sensitive to global warming: The standardized precipitation evapotranspiration index. *J. Climate,* **23,** 1696–1718, doi:10.1175/2009JCLI2909.1.

Wetherald, R. T., and S. Manabe, 2002: Simulation of hydrologic changes associated with global warming. *J. Geophys. Res.,* **107,** 4379, doi:10.1029/2001JD001195.

Wilhite, D. A., and M. H. Glantz, 1985: Understanding the drought phenomenon: The role of definitions. *Water Int.,* **10,** 111–120, doi:10.1080/02508068508686328.

Woodhouse, C. A., J. L. Russell, and E. R. Cook, 2009: Two modes of North American drought from instrumental and paleoclimatic data. *J. Climate,* **22,** 4336–4347, doi:10.1175/2009JCLI2705.1.